Research Article | Vol. 28, No. 20 / 28 September 2020 / Optics Express 29442

Optics EXPRESS

Investigation of electron vortices in time-delayed circularly polarized laser pulses with a semiclassical perspective

SHUAI BEN,[1] SHI CHEN,[2,3] CHENG-RUI BI,[1] JING CHEN,[1,3,5] AND XUE-SHEN LIU[4,6]

[1]*Institute of Applied Physics and Computational Mathematics, P. O. Box 8009, Beijing 100088, China*
[2]*School of Physics, Peking University, Beijing 100871, China*
[3]*HEDPS, Center for Applied Physics and Technology, Peking University, Beijing 100871, China*
[4]*Institute of Atomic and Molecular Physics, Jilin University, Changchun 130012, China*
[5]*chen_jing@iapcm.ac.cn*
[6]*liuxs@jlu.edu.cn*

Abstract: We theoretically investigate strong-filed electron vortices in time-delayed circularly polarized laser pulses by a generalized quantum-trajectory Monte Carlo (GQTMC) model. Vortex interference patterns in photoelectron momentum distributions (PMDs) with various laser parameters can be well reproduced by the semiclassical simulation. The phase difference responsible for the interference structures is analytically identified through trajectory-based analysis and simple-man theory, which reveal the underlying mechanism of electron vortex phenomena for both co-rotating and counter-rotating component. This semiclassical analysis can also demonstrate the influences of laser intensity and wavelength on the number of arms of vortices. Furthermore, we show the influence of the Coulomb effect on the PMDs. Finally, the controlling of the ionization time intervals in the tens to hundreds of attosecond magnitude is qualitatively discussed.

1. Introduction

Photoionization plays a central role in understanding of ultrafast dynamics in atoms and molecules in strong laser fields. Plenty of ultrafast processes are directly related to photoionization, which is the foundation of many strong field phenomena such as high harmonic generation (HHG) and attosecond pulse synthetization [1,2], above threshold ionization (ATI) [3], nonsequential double ionization (NSDI) [4], molecular imaging by laser-assisted photoionization diffraction [5,6]. With the rapid development of laser technology, various kinds of laser pulses have been used in investigation. For example, elliptically or circularly polarized laser pulses have been shown to be important for investigating electron dynamics, such as attoclock technique [7–9], electron angular correlation [10,11], electron recollision in double ionization [12–15] and generation of plasmas in air [16].

Currently, a new kind of synthesized laser pulse with a pair of circularly polarized light is used in strong-field experiment. This scheme was shown first in 1995 that co-rotating or counter-rotating ultrafast circularly polarized pulses with the same or opposite helicities induce recollision of electrons with parent ions [17], and ensuring efficient HHG [18]. The HHG process driven by two-color counter-rotating circularly polarized pulses was shown to span from the extreme ultraviolet (EUV) to the soft x-ray regions of the spectrum and have characteristics of generating phase-matched, bright, circularly polarized harmonics [19–21]. Furthermore, the process of generating polarization-tunable HHG attracts the attention of many scientific researches [20,22,23].

#400846 https://doi.org/10.1364/OE.400846
Journal © 2020 Received 22 Jun 2020; revised 29 Aug 2020; accepted 6 Sep 2020; published 18 Sep 2020

Optics EXPRESS

The circularly polarized synthesized laser fields have also been employed to investigate the strong-field ionization process and to steer ultrafast electron dynamics. For example, the ionization by two-color counter-rotating and co-rotating circularly polarized fields has been studied experimentally and theoretically [24,25]. In the investigations of NSDI dynamics driven by the two-color counter-rotating laser fields, researches showed that the motion of the liberated electron and thus the recollision process can be spatiotemporally manipulated by changing the helicity and relative strength between the two colors [26–30]. In addition, attosecond angular streaking, or the "attoclock" is developed by this kind of bicircular fields [31–34].

Recently, a new phenomenon of electron vortices has attracted much attention. The vortex structures in the PMDs of photoelectron wave packets from the photoionization of atoms with sequences of two time-delayed counter-rotating circularly polarized ultrashort laser pulses were predicted [35] and demonstrated experimentally [36,37].

The shape of vortex and electron angular distributions was shown to be sensitive to the pulse polarization, handedness of two pulses and their time delay. Djiokap *et al*. [35,38] numerically investigated electron vortices with single ionization of He in two ultraviolet (UV) laser pulses, and then further studied single-photon [39] and multiphoton [40] double ionization circumstances. Their researches revealed the effect of laser parameters on the number of the spiral arms in these vortex patterns. Furthermore, a series of investigations of the occurrence of electron vortices in other processes and systems were stimulated. Li *et al*. [41] theoretically investigated the dynamic Stark effect in electron vortices, and revealed the symmetry distortion phenomena. Li *et al*. [42] explored the characterization of the carrier envelope phase of an isolated attosecond pulse by the electron vortex-shaped momentum pattern. Electron vortex phenomena in molecular system were also investigated [43,44], in which the molecular alignment expanded this research scope. Xiao *et al*. [45] proposed and numerically demonstrated a scheme to accurately measure the electron displacement through the interfering vortex photoelectron momentum induced by two time-delayed oppositely circularly polarized laser pulses. Zhen *et al*. [46] investigated the effects of the wavelength and the carrier envelope phase on the vortex structure in details.

In this kind of time-delayed circularly polarized laser pulses, the electron wave packets (EWPs) ionized from an atom at different times with the same final momentum will interfere with each other and show the vortex interference pattern. In previous researches, many few-cycle attosecond pulses with the large bandwidth were used to observe the vortex patterns, in which the electrons ionized through absorbing one or several photons. Accordingly, the vortex patterns also showed several arms. The relationship between the number of photons absorbed, the number of arms and the ionization potential is well explained by the attosecond perturbation ionization theory [47,48].

According to this model, when IR or visible light pluses are used, the number of arms in vortex patterns may be large for low-Z atomic rare gases because of its high ionization potential, which requires a high resolution in experimental measurement. However, few arms may be observed if the high-Z atomic rare gases or metal atom is used because of its lower ionization potential (e.g. atomic potassium used in experimental measurement [36,37]). In this paper, considering laser pulses with wavelength of several hundred nanometers which is easily achieved in experiment and tunneling mechanism in this circumstance, we propose and numerically demonstrate a new scheme with semiclassical perspective to investigate the electron vortices for atomic Xe. Although the attosecond perturbation ionization model succeeds with explaining the phenomena of electron vortices, semiclassical theory can provide a more detailed analysis of the process from a different perspective. With the help of quantum-trajectory description, EWPs interference contributing to vortex pattern can be identified.

This paper is organized as follows. In Sec. II we introduce the GQTMC model and the time-delayed circularly polarized driving field. In Sec. III we present the calculations of PMDs in the synthesized laser pluses. The underlying mechanism of the vortex patterns is discussed based on the statistical trajectory-based analysis and simple-man theory. We summarize our results

Optics EXPRESS

and conclude in Sec. IV. Atomic units (a.u.) are used throughout the paper unless otherwise indicated.

2. Theoretical methods

In order to reveal the physical reason for the electron vortices in a semiclassical perspective, we apply a semiclassical Monte Carlo method to show this interference structures. The quantum trajectory Monte Carlo (QTMC) model [49] is based on the traditional semiclassical model, and Feynman's path-integral approach [50,51]. In this method, each ionized electron trajectory is encoded with a phase , which is given by the action integral along the path. Therefore, this model can simulate the dynamics of EWPs and reproduce the interference patterns. Furthermore, the phase and the asymptotic momentum are nicely modified by Shvetsov-Shilovski *et al*. [52]. Song *et al*. [53] also propose a modified model, so called generalized quantum trajectory Monte Carlo (GQTMC) method, which takes the eect of nonadiabatic ionization into account. In this paper, we apply both of the two modified models.

The details of the GQTMC method are described in [53]. Briefly, the tunneling ionization rate and the initial transverse momentum distribution of electron wave packets are given by the nonadiabatic tunneling ionization theory [54]. The initial longitudinal momentum is neglected. The weight of each trajectory is given by

$$\omega(t_0, \mathbf{v}_{0,\perp}) \propto \Gamma(t_0) \exp\left[-\frac{\sqrt{2I_p}\mathbf{v}_{0,\perp}^2}{E(t_0)}\right], \tag{1}$$

where $\mathbf{v}_{0,\perp}$ is the initial transverse velocity, t_0 is the ionization time, and $\Gamma(t_0)$ is the Yudin-Ivanov formula [54]. After tunneling, the classical motion of the electrons in the combined laser and Coulomb fields is governed by the Newtonian equation,

$$\frac{\mathrm{d}^2}{\mathrm{d}t^2}\mathbf{r} = -\mathbf{E}(\mathbf{t}) - \nabla V(\mathbf{r}), \tag{2}$$

where $\mathbf{E}(\mathbf{t})$ is the laser electric field. $V(\mathbf{r}) = -Z/|\mathbf{r}|$ is the Coulomb potential and Z is the ionic charge. According to [52], the phase of the electron trajectory is given by

$$S_j = -\mathbf{v}_{0,\perp} \cdot \mathbf{r}_j(t_0) + I_p t_0 - \int_{t_0}^{\infty} \left[\frac{\mathbf{p}_j^2(t)}{2} - \frac{2Z}{|\mathbf{r}_j(t)|}\right] dt, \tag{3}$$

in which $\mathbf{r}_j(t_0)$ and $\mathbf{p}_j(t)$ are the initial position and velocity of the jth electron in the combined laser and Coulomb fields, respectively. Accordingly, the phase difference between two trajectories can be defined as $\Delta S = S_1 - S_2$, and the interference patterns are determined by this phase difference, i.e., interference weight $W = \cos^2(\Delta S/2)$.

In our simulation, two hundred million electron trajectories are calculated to obtain the PMDs. The probability of each asymptotic momentum is determined by

$$\left|P(\mathbf{p}_j)\right|^2 = \left|\sum_j \sqrt{\omega_j(t_0, \mathbf{v}_{0,\perp})} \exp\left[-iS_j\right]\right|^2. \tag{4}$$

In the simulation, the synthesized laser pulse with a pair of circularly polarized is written as

$$\mathbf{E}(t) = \mathbf{E}_1(t) + \mathbf{E}_2(t), \tag{5}$$

with

$$\mathbf{E}_1(t) = E_1 f_1(t) \left[\hat{\mathbf{e}}_x \cos(\omega_1 t) + \hat{\mathbf{e}}_y \sin(\omega_1 t)\right], \tag{6}$$

Optics EXPRESS

and

$$\mathbf{E}_2(t) = E_2 f_2(t-\Delta\tau)\ \{\hat{\mathbf{e}}_x \cos[\omega_2(t-\Delta\tau)] \pm \hat{\mathbf{e}}_y \sin[\omega_2(t-\Delta\tau)]\ \}, \tag{7}$$

where ω_i is laser angular frequency. The sign $\pm$ denotes the helicity of (left- or right-handed) circularly polarized laser pulses, which also corresponds to co- or counter-rotating component. $f_i(t) = \exp\left(-4\ln 2t^2/\tau_i^2\right)$ is smooth pulse envelope, and $\tau_i = 2T_i$ indicates full width at half-maximum (FWHM), $T_i = 2\pi/\omega_i$ is one optical cycle (o.c.). Here $i = 1, 2$ represents the laser parameters of the two pulses. $\Delta\tau$ presents the delay time between the two pulses. In order to simplify the analyses in this paper, we fix $\Delta\tau$ the at $3T_1$ for different laser frequency combinations, and the amplitudes of the two laser field E_1 and E_2 are set to the same (fixing the laser intensities at I_0).

3. Results and discussions

In Fig. 1 we display the simulated results of PMDs for atomic Xe by the synthesized laser pulses with counter-rotating (upper panel) and co-rotating (lower panel) components. Various laser parameters are used to enhance the universality, e.g., the wavelengths $\lambda_1 = \lambda_2 = 260$ nm and $I_0 = 0.09$ PW/cm^2 in Fig. 1(a); $\lambda_1 = 320$ nm, $\lambda_2 = 250$ nm, and $I_0 = 0.09$ PW/cm^2 in Fig. 1(b); $\lambda_1 = \lambda_2 = 400$ nm and $I_0 = 0.058$ PW/cm^2 in Fig. 1(c); $\lambda_1 = 500$ nm, $\lambda_2 = 450$ nm, and $I_0 = 0.075$ PW/cm^2 in Fig. 3(d); $\lambda_1 = 450$ nm, $\lambda_2 = 340$ nm, and $I_0 = 0.08$ PW/cm^2 in Fig. 1(e); $\lambda_1 = 480$ nm, $\lambda_2 = 300$ nm, and $I_0 = 0.07$ PW/cm^2 in Fig. 1(f). Overall, all of the PMDs in Fig. 1 show the clear vortex interference patterns. Altering the laser parameters also varies the spiral bursts in PMDs. The number of the arms in vortices changes from 6 to 10 for the co-rotating case, whereas it changes from 1 to 3 for counter-rotating case. The dependence of the number of the arms on the laser wavelengths and intensities indicates the essential role of the combined vector fields in driving EWPs to spiral away with different rotate speeds and directions, which leads to various interference processes.

To further show the origin of vortex interferences, we trace the trajectories of the electrons which interfere with each other and form the arms of the vortex. Typical trajectories are selected from areas at the arms of the vortices as shown in Fig. 2. The selected areas are marked by P1 (for counter-rotating case) and P2 (for co-rotating case), respectively [shown in Figs. 1(b) and (e)]. The red lines show the two kinds of typical ionization trajectories that have the same final momenta in counter-rotating components. It is easy to see the longer ionization trajectory is generated by the first laser field $\mathbf{E}_1(t)$, and shorter one is generated by the delayed field $\mathbf{E}_2(t)$. The longer trajectory firstly spirals in anti-clockwise direction and then turns to spiral away clockwise because it is successively driven by the counter-rotating circularly polarized laser pulses, while the shorter trajectory merely spirals away clockwise in the delayed laser pulse. The dashed line part in longer trajectory shows the major path difference between the two trajectories, which includes the path in both $\mathbf{E}_1(t)$ and $\mathbf{E}_2(t)$. In solid line part, the path shape of longer trajectory tends to be similar to the path shape of shorter trajectory and they have coincident final states at last. Therefore, it is believed that this path difference along the dashed line part is substantially responsible for the phase difference ΔS and leads to forming the interference arms of the vortex structures.

The case of co-rotating is similar (blue lines in Fig. 2). The longer trajectory always spirals in anti-clockwise direction because the driven pluses have the same helicity, and then it tends to be coincident with the shorter trajectory. However, the amplitude of rotation decreases when it is driven by the delayed laser pulse in turn because it has a shorter wavelength. Similarly, the dashed line part shows the major path difference responsible for the phase difference ΔS.

Based on the above analysis, we further calculate ΔS in the framework of the simple-man theory, in which the electron responds only to the laser field. This model has been repeatedly applied in discussions of strong-field ionization. In this model, the Coulomb potential and the initial

Optics EXPRESS

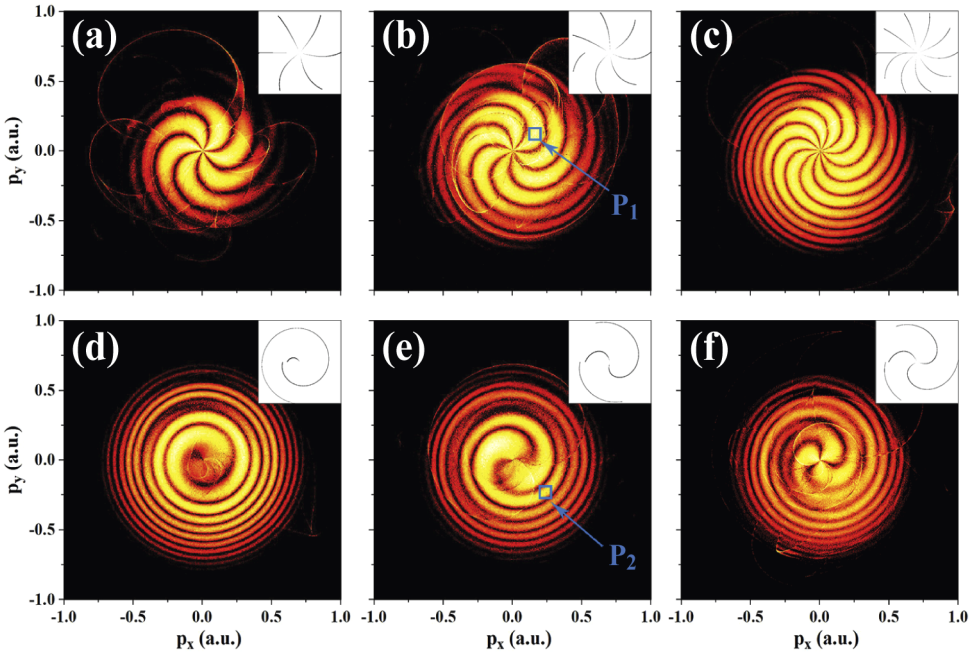

Fig. 1. Simulated PMDs for atomic Xe by the synthesized laser pulses with counter-rotating (upper panel) and co-rotating (lower panel) components by QTMC method at laser parameters of (a) $\lambda_1 = \lambda_2 = 260$ nm and $I_0 = 0.09$ PW/cm^2; (b) $\lambda_1 = 320$ nm, $\lambda_2 = 250$ nm, and $I_0 = 0.09$ PW/cm^2; (c) $\lambda_1 = \lambda_2 = 400$ nm and $I_0 = 0.058$ PW/cm^2; (d) $\lambda_1 = 500$ nm, $\lambda_2 = 450$ nm, and $I_0 = 0.075$ PW/cm^2; (e) $\lambda_1 = 450$ nm, $\lambda_2 = 340$ nm, and $I_0 = 0.08$ PW/cm^2; (f)$\lambda_1 = 480$ nm, $\lambda_2 = 300$ nm, and $I_0 = 0.07$ PW/cm^2. Inset: calculated curves by Eq. (28) corresponding to the PMDs with same laser parameters. The curves show clear spiral shapes and have the same arm-numbers of the corresponding PMDs.

longitudinal momentum are neglected. We simplify the external field as two sequential single-cycle circularly polarized laser fields without carrier envelope as follows (the counter-rotating case):

$$\mathbf{E}_1^-(t) = E_{x,1}(t)\hat{\mathbf{e}}_x + E_{y,1}(t)\hat{\mathbf{e}}_y, \tag{8}$$

and

$$\mathbf{E}_2^-(t) = E_{x,2}(t)\hat{\mathbf{e}}_x + E_{y,2}(t)\hat{\mathbf{e}}_y, \tag{9}$$

with

$$E_{x,1}(t) = E_1 \cos(\omega_1 t), \tag{10}$$

$$E_{y,1}(t) = E_1 \sin(\omega_1 t), \tag{11}$$

$$E_{x,2}(t) = -E_2 \cos(\omega_2 t), \tag{12}$$

$$E_{y,2}(t) = E_2 \sin(\omega_2 t), \tag{13}$$

The first electron with longer trajectory is born in $\mathbf{E}_1^-(t)$ while the second electron with shorter trajectory is born in $\mathbf{E}_2^-(t)$. The birth time of each trajectory is defined as t_1 and t_2, respectively. We assume that the first electron has the same path with the other from t_2 and interferes with it at the final time of $\mathbf{E}_2^-(t)$. Therefore, the ΔS is determined by the path where the first electron moves from t_1 to t_2.

Optics EXPRESS

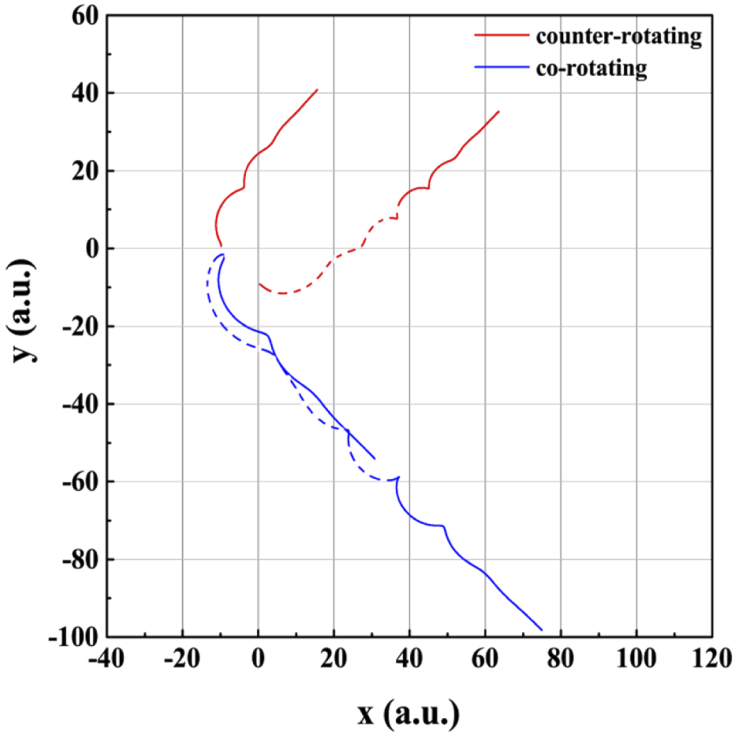

Fig. 2. Typical trajectories responsible for the vortex structures in the PMDs. Red (blue) lines show the trajectories in counter-rotating (co-rotating) case selected from the areas marked by P1 (P2) in Fig. 3. The dashed lines show the parts of path differences between two kinds of ionization trajectories, which are mainly contributed to the phase difference ΔS and lead to the interference patterns.

According to $\mathbf{p}(t) = \mathbf{p}_0 - \mathbf{A}(t)$ [$\mathbf{A}(t)$ is the laser field's vector potential and $\mathbf{p}_0$ is the initial transverse momentum], the final momenta of two electrons are

$$\mathbf{p}_1^f(t_1) = p_{x,1}^f(t_1)\hat{\mathbf{e}}_x + p_{y,1}^f(t_1)\hat{\mathbf{e}}_y, \tag{14}$$

and

$$\mathbf{p}_2^f(t_2) = p_{x,2}^f(t_2)\hat{\mathbf{e}}_x + p_{y,2}^f(t_2)\hat{\mathbf{e}}_y, \tag{15}$$

with

$$p_{x,1}^f(t_1) = \frac{E_1}{\omega_1}\sin(\omega_1 t_1) + p_{0,x1}, \tag{16}$$

$$p_{y,1}^f(t_1) = -\frac{E_1}{\omega_1}\cos(\omega_1 t_1) + p_{0,y1}, \tag{17}$$

$$p_{x,2}^f(t_2) = -\frac{E_2}{\omega_2}\sin(\omega_2 t_2) + p_{0,x2}, \tag{18}$$

$$p_{y,2}^f(t_2) = -\frac{E_2}{\omega_2}\cos(\omega_2 t_2) + p_{0,y2}. \tag{19}$$

Letting $\mathbf{p}_1^f(t_1) = \mathbf{p}_2^f(t_2)$ we can get the initial ionization time condition for interference in the case of counter-rotating. Note that the initial transverse velocities are always parallel with the final momentum and have a range of distribution. As a consequence, the initial transverse momenta

Optics EXPRESS

can arbitrarily compensate the drift momenta $E_i/\omega_i (i = 1, 2)$ if the difference between the two drift momenta is not too much. Therefore we can assume that the final momenta have the same magnitude and the ionization time condition can be written as

$$\omega_1 t_1 + \omega_2 t_2 = 2\pi N,\ N = 0,\ \pm 1,\ \pm 2 \cdots \tag{20}$$

The electron motion responsible for the phase difference is regard as being separated into two steps in $\mathbf{E}_1^-(t)$ and $\mathbf{E}_2^-(t)$. Accordingly, the phase differences in the two steps are defined as ΔS_1 and ΔS_2. Considering the above analyses we rewrite the phase difference as

$$\Delta S = \Delta S_1 + \Delta S_2, \tag{21}$$

with

$$\Delta S_1 = \frac{1}{2}\int_{t_1}^{T_1} \left[p_{x,1}^2(t) + p_{y,1}^2(t)\right] dt + I_p(T_1 - t_1), \tag{22}$$

$$\Delta S_2 = \frac{1}{2}\int_{0}^{t_2} \left[p_{x,2}^2(t) + p_{y,2}^2(t)\right] dt + I_p t_2. \tag{23}$$

The electron momenta in $\mathbf{E}_1^-(t)$ and $\mathbf{E}_2^-(t)$ can be expressed as

$$p_{x,1}(t) = p_{0,x1} - \int_{t_1}^{t} E_{x,1}(\tau)\, d\tau = p_{0,x1} - \frac{1}{\omega_1}\left[E_{y,1}(t) - E_{y,1}(t_1)\right], \tag{24}$$

$$p_{y,1}(t) = p_{0,y1} - \int_{t_1}^{t} E_{y,1}(\tau)\, d\tau = p_{0,y1} + \frac{1}{\omega_1}\left[E_{x,1}(t) - E_{x,1}(t_1)\right], \tag{25}$$

and

$$p_{x,2}(t) = p_{x,1}^f(t_1) - \int_{0}^{t_2} E_{x,2}(\tau)\, d\tau = p_{x,1}^f(t_1) + \frac{1}{\omega_2} E_{y,2}(t), \tag{26}$$

$$p_{y,2}(t) = p_{y,1}^f(t_1) - \int_{0}^{t_2} E_{y,2}(\tau)\, d\tau = p_{y,1}^f(t_1) - \frac{1}{\omega_2} E_{x,2}(t). \tag{27}$$

Then the Eq. (21) can be reduced to

$$\Delta S = \frac{1}{2}\left(p_f^2 + \frac{E_1^2}{\omega_1^2}\right)(T_1 - t_1) + \frac{1}{2}\left(p_f^2 + \frac{E_2^2}{\omega_2^2}\right) t_2 + I_p(T_1 - t_1) + I_p t_2, \tag{28}$$

where $p_f = \left|\mathbf{p}_1^f(t_1)\right| = \left|\mathbf{p}_2^f(t_2)\right|$ is the magnitude of final momentum in PMDs. Equation (28) is the analytic form of the phase difference in the interference structures. Fixing the interference weight W and taking the initial condition Eq. (20) into account, we find that the electron momentum monotonically changes versus the rotation angle $\omega_1 t_1$ (or $\omega_2 t_2$), which exactly shows the spiral interference patterns. We picture the curves of momentum that makes $W = 1$ when the rotation angle $\omega_1 t_1$ changes in one cycle (e.g. t_1 changes from 0 to T_1) as shown in illustrations in Fig. 1. The curves visually show the vortex patterns of corresponding PMDs.

The restrictive condition $W = 1$ corresponds to the interference maxima, in which the $\Delta S/2$ should be an integer multiple of π. Because the ΔS monotonically changes versus t_1, the number of interference maxima in one cycle can be defined by the multiple changing with $\Delta S/2$ in one optical cycle. Therefore, we regard the ΔS as a function of t_1 i.e. $\Delta S(t_1)$, and the number of the arms of vortex structures in the case of counter-rotating can be estimated by

$$N^- = \frac{1}{2\pi}\left|\Delta S(0) - \Delta S(T_1)\right|, \tag{29}$$

with the initial condition Eq. (20).

Optics EXPRESS

Assuming $p_f = E_1/\omega_1$ according to the simple-man theory, and bringing the laser parameters used in Figs. 1(a), (b) and (c) into Eq. (29), we can approximately calculate the corresponding number of the arms $N^- = 6,\ 7$ and 10. The results are in good agreement with the PMDs calculated by GQTMC methods.

Similarly, the external field for co-rotating case can be simplified as

$$\mathbf{E}_1^+(t) = E_{x,1}(t)\hat{\mathbf{e}}_x + E_{y,1}(t)\hat{\mathbf{e}}_y, \tag{30}$$

and

$$\mathbf{E}_2^+(t) = E_{x,2}(t)\hat{\mathbf{e}}_x + E_{y,2}(t)\hat{\mathbf{e}}_y, \tag{31}$$

with

$$E_{x,1}(t) = E_1 \cos(\omega_1 t), \tag{32}$$

$$E_{y,1}(t) = E_1 \sin(\omega_1 t), \tag{33}$$

$$E_{x,2}(t) = E_2 \cos(\omega_2 t), \tag{34}$$

$$E_{y,2}(t) = E_2 \sin(\omega_2 t), \tag{35}$$

and then the final momentum of two electrons are given by

$$p_{x,1}^f(t_1) = \frac{E_1}{\omega_1}\sin(\omega_1 t_1) + p_{0,x1}, \tag{36}$$

$$p_{y,1}^f(t_1) = -\frac{E_1}{\omega_1}\cos(\omega_1 t_1) + p_{0,y1}, \tag{37}$$

$$p_{x,2}^f(t_2) = \frac{E_2}{\omega_2}\sin(\omega_2 t_2) + p_{0,x2}, \tag{38}$$

$$p_{y,2}^f(t_2) = -\frac{E_2}{\omega_2}\cos(\omega_2 t_2) + p_{0,y2}. \tag{39}$$

We also let $\mathbf{p}_1^f(t_1) = \mathbf{p}_2^f(t_2)$. The initial ionization time condition for co-rotating case is obtained

$$\omega_1 t_1 - \omega_2 t_2 = 2\pi N,\ N = 0,\ \pm 1,\ \pm 2 \cdots \tag{40}$$

Interestingly, this condition shows that the two electrons always release at the same tunneling site as shown in Fig. 2. The two blue lines have the same starting point.

We do a similar procedure as used in counter-rotating case, and find that the ΔS in co-rotating case has the same form with Eq. (28). Therefore, the number of the arms can be estimated by

$$N^+ = \frac{1}{2\pi}\left|\Delta S(0) - \Delta S(T_1)\right|, \tag{41}$$

but with the initial condition Eq. (40).

Bringing the laser parameters used in Figs. 1(d), (e) and (f) into Eq. (28), we can approximately calculate the corresponding number of the arms $N^+ = 1,\ 2$ and 3 for co-rotating case, which are also coincident with the results calculated by GQTMC method.

The analytical explanation is obtained according to the simple-man theory, which contains substantial approximate treatment. It neglects the effect of Coulomb potential, the initial longitudinal momentum and the carrier envelope, which could lead to deviations. For example, the curvatures of arms are not uniform and contain some disconnected lines. Furthermore, the effect of delay time is not shown in this paper, which demands further explorations. However, the analyses reproduce the vortex interference structures in PMDs and directly reveal the mechanisms of electron vortex phenomena.

Optics EXPRESS

In addition, the description of classical theory is qualitatively consistent with quantum mechanics. For example, when applying two lasers combined with a wavelength of several hundred nanometers, the external counter-rotating drive field will cause a relative increase in the number of arms. Conversely, the external co-rotating drive field will result in fewer arms. This can be explained from the initial conditions of ionization time. Condition Eq. (20) shows that changes in t_1 and t_2 will cause ΔS_1 and ΔS_2 to have the same tendency, and thus increase the magnitude of the total phase difference ΔS. Therefore, a larger value of N^+ will be obtained. On the contrary, condition Eq. (40) corresponds to an opposite result. This conclusion is qualitatively consistent with quantum theory [38,43].

In the quantum description, different multi-photon processes are explained by the attosecond perturbation ionization model. For example, Yuan *et al*. show that the number of the arms in spiral interference patterns is dependent on the sum of the numbers of absorbed photons in the two laser pulse for counter-rotating case, while the number of the arms is dependent on the difference between the numbers of absorbed photons for co-rotating case [43]. Similarly, the external counter-rotating drive field will cause more arms while the external co-rotating drive field will result in fewer arms quantity.

This semiclassical model can also easily show some other details of the physical processes under the vortex structures. For example, the Coulomb effects can be discussed by turning on or turning off the Coulomb potential of each trajectory. In Fig. 3(a), we show the PMD with the same laser parameters as in Fig. 1(b) but turn off the Coulomb potential. This Coulomb-free simulation result also shows the similar vortex interference patterns, but there are two main differences caused by the Coulomb effects. (1) It shows a rotation of the vortex structure as compared to the simulation including the ionic potential [Fig. 1(b)]. The rotation can be clearly seen in the polar plots of photoelectron angular distributions as shown in the illustration, where black (red) line shows the result with (without) considering Coulomb potential. Because the rotation is mainly reflected on the arms of the vortex patterns, we only count the angular distributions with corresponding momenta larger than 0.15. The Coulomb attraction deflects the spiral motion of electrons and causes the rotation phenomenon, which widely exists in strong field ionization driven by circularly or elliptically polarized laser fields [27,55,56]. (2) There is an evident enhancement in the center of the PMD. The reason is that the Coulomb-free system overestimates the yields of electrons that should be recaptured by the Coulomb attraction in the system including the ionic potential (frustrated ionization [57]).

If we just turn off the long-range Coulomb potential only after the end of the laser pulse (without an analytical asymptotic), the result shows a hole in the center of the PMD as shown in Fig. 3(b), which means absence of low-energy distribution caused by the long-range Coulomb eect (also called the Coulomb potential tail effect). Modified model [52] of QTMC considered in this paper modifies the phase and the asymptotic momentum. Therefore, the simulated PMDs including the Coulomb potential show a complete low-energy distribution.

Unlike the case in an elliptically polarized laser field that leads to a significant asymmetry in the PMD, the major part of the vortex structures cannot be distorted by the Coulomb attraction due to the rotational symmetry in a circularly polarized laser field. As a consequence, it is believed that the vortex interference structures are mainly dependent on the initial states of the tunneled electrons and the drive laser field, and the influence of Coulomb potential is relatively suppressed. This result may offer a feasible method to investigate that the initial states can be mapped onto the PMDs of electron vortices.

It can be seen from the analytical formula that the total phase difference depends on laser parameters such as laser intensity and atomic ionization potential. Changes in these parameters can cause changes in the number of arms in the vortex structure. This analysis helps us to estimate the information of ionization time, and the interval between the arms (stripe spacing) can map the corresponding interval of ionization time. For example, when using the counter-rotating laser

Optics EXPRESS

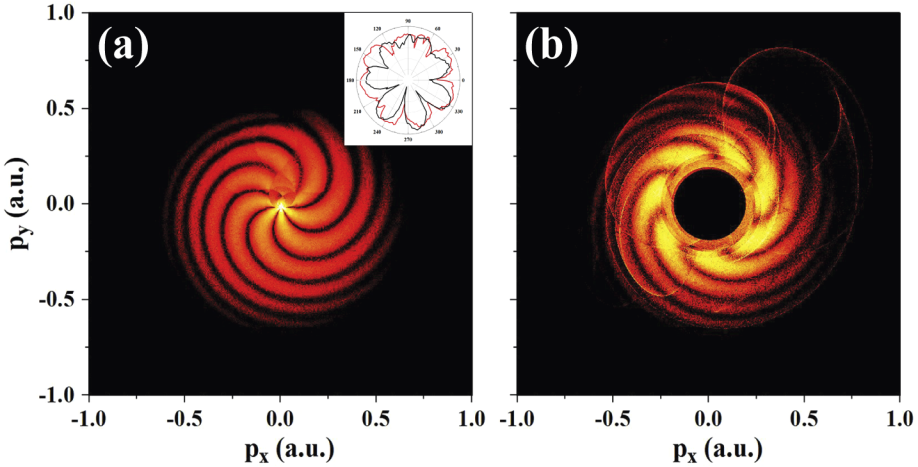

Fig. 3. The influence of the Coulomb effects on PMDs. (a) The Coulomb-free simulation. Inset: the polar plots of photoelectron angular distributions, where black (red) line shows the result with (without) considering Coulomb potential. (b) The simulation with only turning off the Coulomb potential after the end of the laser pulse. The laser parameters are identical to those of Fig. 3(b).

field with the same laser parameters as in Fig. 3(c), the interval of ionization time corresponding to fringe spacing can be estimate by $\Delta t = T_1/N^- \simeq 132$ attoseconds. If only the laser intensity is increased to 0.16 PW/cm^2 (the other parameters remain unchanged), the ionization time interval becomes about 95 attoseconds; if only the target atoms are changed, such as the Ne atom with an ionization potential of 0.792, the time interval is about 82 attoseconds. Therefore, we may control the time intervals in the tens to hundreds of attosecond magnitude by tuning the laser parameters or choosing different target atoms.

Furthermore, the analytical model can offer other feasible plans of extended researches. For example, the electron-ion rescattering process can be investigated in the electron vortex phenomena. As we known, the rescattering in double ionization of magnesium by the circularly polarized laser fields has been explored both experimentally and theoretically [12,13,15]. According to Eq (28), the electrons released time can be related to the arms of the vortex structures. In the ionization of atomic magnesium by the time-delayed circularly polarized laser pulses, the time of rescattering could be mapped onto the vortex interference patterns in PMDs. Therefore, the rescattering time in circular polarization may also be investigated in several tens or several hundreds of attosecond magnitude in this analytical model.

4. Conclusion

In conclusion, we theoretically investigate the electron vortex phenomena by GQTMC method. Clear vortex structures in PMDs are well reproduced. With the help of semiclassical analysis, typical trajectories responsible for the vortex interference patterns are identified, from which we can find that the phase difference contributed to the interference is derived from the path difference between two photoelectron wave packets induced by the two sequential laser pulses. The phase difference can be analytically calculated by the simple-man theory. The results demonstrate that the vortex structures are influenced by laser intensities and wavelengths. The number of arms of the vortices can also be determined for both co-rotating and counter-rotating component. Based on a semiclassical perspective, which is different from the quantum theory,

Optics EXPRESS

our study presents a clear physical picture of the electron vortex phenomena and helps ones to explore underlying physics from a different point of view.

Funding

National Key Research and Development Program of China (2016YFA0401100, 2019YFA0307700).

Disclosures

The authors declare no conflicts of interest.

References

1. F. Krausz and M. Ivanov, "Attosecond physics," Rev. Mod. Phys. **81**(1), 163–234 (2009).
2. Z. Chang and P. Corkum, "Attosecond photon sources: the first decade and beyond," J. Opt. Soc. Am. B **27**(11), B9 (2010).
3. W. Becker, F. Grasbon, R. Kopold, D. Milošević, G. Paulus, and H. Walther, "Above-threshold ionization: from classical features to quantum effects," Adv. At. Mol. Opt. Phys. **48**, 35–98 (2002).
4. W. Becker, X. Liu, P. Ho, and J. H. Eberly, "Theories of photoelectron correlation in laser-driven multiple atomic ionization," Rev. Mod. Phys. **84**(3), 1011–1043 (2012).
5. M. Meckel, D. Comtois, D. Zeidler, A. Staudte, D. Pavičić, H. C. Bandulet, H. Pépin, J. C. Kieffer, R. Dörner, D. M. Villeneuve, and P. B. Corkum, "Laser-induced electron tunneling and diffraction," Science **320**(5882), 1478–1482 (2008).
6. C. I. Blaga, J. Xu, E. S. A. D. Dichiara, K. Zhang, P. Agostini, T. A. Miller, L. F. DiMauro, and C. D. Lin, "Imaging ultrafast molecular dynamics with laser-induced electron diffraction," Nature (London) **483**(7388), 194–197 (2012).
7. P. Eckle, M. Smolarski, P. Schlup, J. Biegert, A. Staudte, M. Schöffler, H. G. Muller, R. Dörner, and U. Keller, "Attosecond angular streaking," Nat. Phys. **4**(7), 565–570 (2008).
8. P. Eckle, A. N. Pfeiffer, C. Cirelli, A. Staudte, R. Dörner, H. G. Muller, M. Büttiker, and U. Keller, "Attosecond ionization and tunneling delay time measurements in helium," Science **322**(5907), 1525–1529 (2008).
9. L. Torlina, F. Morales, J. Kaushal, I. Ivanov, A. Kheifets, A. Zielinski, A. Scrinzi, H. G. Muller, S. Sukiasyan, M. Ivanov, and O. Smirnova, "Interpreting attoclock measurements of tunnelling times," Nat. Phys. **11**(6), 503–508 (2015).
10. J. T. X. Wang and J. H. Eberly, "Angular correlation in strong-field double ionization under circular polarization," Phys. Rev. Lett. **110**(7), 073001 (2013).
11. S. Ben, P.-Y. Guo, K.-L. Song, T.-T. Xu, W.-W. Yu, and X.-S. Liu, "Nonsequential double ionization of Mg from a doubly excited complex driven by circularly polarized laser field," Opt. Express **25**(2), 1288 (2017).
12. F. Mauger, C. Chandre, and T. Uzer, "Recollisions and correlated double ionization with circularly polarized light," Phys. Rev. Lett. **105**(8), 083002 (2010).
13. A. Kamor, F. Mauger, C. Chandre, and T. Uzer, "How key periodic orbits drive recollisions in a circularly polarized laser field," Phys. Rev. Lett. **110**(25), 253002 (2013).
14. S. Ben, T. Wang, T. Xu, J. Guo, and X. Liu, "Nonsequential double ionizationchannels control of Ar with few-cycle elliptically polarized laser pulse by carrier-envelope-phase," Opt. Express **24**(7), 7525 (2016).
15. Y. H. Lai, X. Wang, Y. Li, X. Gong, B. K. Talbert, C. I. Blaga, P. Agostini, and L. F. DiMauro, "Experimental test of recollision effects in double ionization of magnesium by near-infrared circularly polarized fields," Phys. Rev. A **101**(1), 013405 (2020).
16. S. Mitryukovskiy, Y. Liu, P. Ding, A. Houard, A. Couairon, and A. Mysyrowicz, "Plasma luminescence from femtosecond filaments in air: Evidence for impact excitation with circularly polarized light pulses," Phys. Rev. Lett. **114**(6), 063003 (2015).
17. T. Zuo and A. D. Bandrauk, "High-order harmonic generation in intense laser and magnetic fields," J. Nonlinear Opt. Phys. Mater. **04**(03), 533–546 (1995).
18. A. D. Bandrauk and H. Lu, "Controlling harmonic generation in molecules with intense laser and static magnetic fields: Orientation effects," Phys. Rev. A **68**(4), 043408 (2003).
19. H. Eichmann, A. Egbert, S. Nolte, C. Momma, B. Wellegehausen, W. Becker, S. Long, and J. K. McIver, "Polarization-dependent high-order two-color mixing," Phys. Rev. A **51**(5), R3414–R3417 (1995).
20. A. Fleischer, O. Kfir, T. Diskin, P. Sidorenko, and O. Cohen, "Spin angular momentum and tunable polarization in high-harmonic generation," Nat. Photonics **8**(7), 543–549 (2014).
21. O. Kfir, P. Grychtol, E. Turgut, R. Knut, D. Zusin, D. Popmintchev, T. Popmintchev, H. Nembach, J. M. Shaw, A. Fleischer, H. Kapteyn, M. Murnane, and O. Cohen, "Generation of bright phase-matched circularly-polarized extreme ultraviolet high harmonics," Nat. Photonics **9**(2), 99–105 (2015).
22. K. M. Dorney, J. L. Ellis, C. Hernández-García, D. D. Hickstein, C. A. Mancuso, N. Brooks, T. Fan, G. Fan, D. Zusin, C. Gentry, P. Grychtol, H. C. Kapteyn, and M. M. Murnane, "Helicity-selective enhancement and polarization control of attosecond high harmonic waveforms driven by bichromatic circularly polarized laser fields," Phys. Rev. Lett. **119**(6), 063201 (2017).

Optics EXPRESS

23. J. Heslar, D. A. Telnov, and S.-I. Chu, "Conditions for perfect circular polarization of high-order harmonics driven by bichromatic counter-rotating laser fields," Phys. Rev. A **99**(2), 023419 (2019).
24. C. A. Mancuso, D. D. Hickstein, P. Grychtol, R. Knut, O. Kfir, X.-M. Tong, F. Dollar, D. Zusin, M. Gopalakrishnan, C. Gentry, E. Turgut, J. L. Ellis, M.-C. Chen, A. Fleischer, O. Cohen, H. C. Kapteyn, and M. M. Murnane, "Strong-field ionization with two-color circularly polarized laser fields," Phys. Rev. A **91**(3), 031402 (2015).
25. C. A. Mancuso, K. M. Dorney, D. D. Hickstein, J. L. Chaloupka, X.-M. Tong, J. L. Ellis, H. C. Kapteyn, and M. M. Murnane, "Observation of ionization enhancement in two-color circularly polarized laser fields," Phys. Rev. A **96**(2), 023402 (2017).
26. C. A. Mancuso, K. M. Dorney, D. D. Hickstein, J. L. Chaloupka, J. L. Ellis, F. J. Dollar, R. Knut, P. Grychtol, D. Zusin, C. Gentry, M. Gopalakrishnan, H. C. Kapteyn, and M. M. Murnane, "Controlling nonsequential double ionization in two-color circularly polarized femtosecond laser fields," Phys. Rev. Lett. **117**(13), 133201 (2016).
27. S. Eckart, M. Richter, M. Kunitski, A. Hartung, J. Rist, K. Henrichs, N. Schlott, H. Kang, T. Bauer, H. Sann, L. P. H. Schmidt, M. Schöffler, T. Jahnke, and R. Dörner, "Nonsequential double ionization by counterrotating circularly polarized two-color laser fields," Phys. Rev. Lett. **117**(13), 133202 (2016).
28. K. Lin, X. Jia, Z. Yu, F. He, J. Ma, H. Li, X. Gong, Q. Song, Q. Ji, W. Zhang, H. Li, P. Lu, H. Zeng, J. Chen, and J. Wu, "Comparison study of strong-field ionization of molecules and atoms by bicircular two-color femtosecond laser pulses," Phys. Rev. Lett. **119**(20), 203202 (2017).
29. X. Ma, Y. Zhou, Y. Chen, M. Li, Y. Li, Q. Zhang, and P. Lu, "Timing the release of the correlated electrons in strong-field nonsequential double ionization by circularly polarized two-color laser fields," Opt. Express **27**(3), 1825 (2019).
30. C. Huang, H. Pang, X. Huang, M. Zhong, and Z. Wu, "Relative phase effect of nonsequential double ionization of molecules by counter-rotating two-color circularly polarized fields," Opt. Express **28**(7), 10505 (2020).
31. M. Han, P. Ge, Y. Shao, Q. Gong, and Y. Liu, "Attoclock photoelectron interferometry with two-color corotating circular fields to probe the phase and the amplitude of emitting wave packets," Phys. Rev. Lett. **120**(7), 073202 (2018).
32. P. Ge, M. Han, Y. Deng, Q. Gong, and Y. Liu, "Universal description of the attoclock with two-color corotating circular fields," Phys. Rev. Lett. **122**(1), 013201 (2019).
33. N. Eicke and M. Lein, "Attoclock with counter-rotating bicircular laser fields," Phys. Rev. A **99**(3), 031402 (2019).
34. M. Han, P. Ge, Y. Fang, X. Yu, Z. Guo, X. Ma, Y. Deng, Q. Gong, and Y. Liu, "Unifying tunneling pictures of strong-field ionization with an improved attoclock," Phys. Rev. Lett. **123**(7), 073201 (2019).
35. J. M. N. Djiokap, S. X. Hu, L. B. Madsen, N. L. Manakov, A. V. Meremianin, and A. F. Starace, "Electron vortices in photoionization by circularly polarized attosecond pulses," Phys. Rev. Lett. **115**(11), 113004 (2015).
36. D. Pengel, S. Kerbstadt, D. Johannmeyer, L. Englert, T. Bayer, and M. Wollenhaupt, "Electron vortices in femtosecond multiphoton ionization," Phys. Rev. Lett. **118**(5), 053003 (2017).
37. J. M. N. Djiokap, A. V. Meremianin, N. L. Manakov, S. X. Hu, L. B. Madsen, and A. F. Starace, "Multistart spiral electron vortices in ionization by circularly polarized uv pulses," Phys. Rev. A **94**(1), 013408 (2016).
38. D. Pengel, S. Kerbstadt, L. Englert, T. Bayer, and M. Wollenhaupt, "Control of three-dimensional electron vortices from femtosecond multiphoton ionization," Phys. Rev. A **96**(4), 043426 (2017).
39. J. M. N. Djiokap, A. V. Meremianin, N. L. Manakov, S. X. Hu, L. B. Madsen, and A. F. Starace, "Kinematical vortices in double photoionization of helium by attosecond pulses," Phys. Rev. A **96**(1), 013405 (2017).
40. J. M. N. Djiokap and A. F. Starace, "Doubly-excited state effects on two-photon double ionization of helium by time-delayed, oppositely circularly-polarized attosecond pulses," J. Opt. **19**(12), 124003 (2017).
41. M. Li, G. Zhang, X. Kong, T. Wang, X. Ding, and J. Yao, "Dynamic stark induced vortex momentum of hydrogen in circular fields," Opt. Express **26**(2), 878 (2018).
42. M. Li, G. Zhang, X. Ding, and J. Yao, "Carrier envelope phase description for an isolated attosecond pulse by momentum vortices," Chin. Phys. Lett. **36**(6), 063201 (2019).
43. K.-J. Yuan, S. Chelkowski, and A. D. Bandrauk, "Photoelectron momentum distributions of molecules in bichromatic circularly polarized attosecond uv laser fields," Phys. Rev. A **93**(5), 053425 (2016).
44. J. M. N. Djiokap, A. V. Meremianin, N. L. Manakov, L. B. Madsen, S. X. Hu, and A. F. Starace, "Dynamical electron vortices in attosecond double photoionization of H_2," Phys. Rev. A **98**(6), 063407 (2018).
45. X.-R. Xiao, M.-X. Wang, H. Liang, Q. Gong, and L.-Y. Peng, "Proposal for measuring electron displacement induced by a short laser pulse," Phys. Rev. Lett. **122**(5), 053201 (2019).
46. Q. Zhen, H.-D. Zhang, S.-Q. Zhang, L. Ji, T. Han, and X.-S. Liu, "Generation of electron vortices in photoionization by counter-rotating circularly polarized attosecond pulses," Chem. Phys. Lett. **738**, 136885 (2020).
47. E. A. Pronin, A. F. Starace, M. V. Frolov, and N. L. Manakov, "Perturbation theory analysis of attosecond photoionization," Phys. Rev. A **80**(6), 063403 (2009).
48. E. A. Pronin, A. F. Starace, and L. Y. Peng, "Perturbation-theory analysis of ionization by a chirped few-cycle attosecond pulse," Phys. Rev. A **84**(1), 013417 (2011).
49. M. Li, J.-W. Geng, H. Liu, Y. Deng, C. Wu, L.-Y. Peng, Q. Gong, and Y. Liu, "Classical-quantum correspondence for above-threshold ionization," Phys. Rev. Lett. **112**(11), 113002 (2014).
50. R. P. Feynman, "Space-time approach to non-relativistic quantum mechanics," Rev. Mod. Phys. **20**(2), 367–387 (1948).

Optics EXPRESS

51. P. Saliéres, B. Carré, L. L. Déroff, F. Grasbon, G. G. Paulus, H. Walther, R. Kopold, W. Becker, D. B. Milošević, A. Sanpera, and M. Lewenstein, "Feynman's path-integral approach for intense-laser–atom interactions," Science **292**(5518), 902–905 (2001).
52. N. I. Shvetsov-Shilovski, M. Lein, L. Madsen, E. Räsänen, C. Lemell, J. Burgdörfer, D. Arbó, and K. Tőkési, "Semiclassical two-step model for strong-field ionization," Phys. Rev. A **94**(1), 013415 (2016).
53. X. Song, C. Lin, Z. Sheng, P. Liu, Z. Chen, W. Yang, S. Hu, C. D. Lin, and J. Chen, "Unraveling nonadiabatic ionization and coulomb potential eect in strong-feld photoelectron holography," Sci. Rep. **6**(1), 28392 (2016).
54. G. L. Yudin and M. Y. Ivanov, "Nonadiabatic tunnel ionization: Looking inside a laser cycle," Phys. Rev. A **64**(1), 013409 (2001).
55. M. Spanner, S. Gräfe, S. Chelkowski, D. Pavičić, M. Meckel, D. Zeidler, A. B. Bardon, B. Ulrich, A. D. Bandrauk, D. M. Villeneuve, R. Dörner, P. B. Corkum, and A. Staudte, "Coulomb asymmetry and sub-cycle electron dynamics in multiphoton multiple ionization of H_2," J. Phys. B **45**(19), 194011 (2012).
56. M. Li, Y. Liu, H. Liu, Q. Ning, L. Fu, J. Liu, Y. Deng, C. Wu, L. Peng, and Q. Gong, "Subcycle dynamics of coulomb asymmetry in strong elliptical laser fields," Phys. Rev. Lett. **111**(2), 023006 (2013).
57. T. Nubbemeyer, K. Gorling, A. Saenz, U. Eichmann, and W. Sandner, "Strong-field tunneling without ionization," Phys. Rev. Lett. **101**(23), 233001 (2008).